Kinematic analysis of MacPherson strut suspension system

Conference Paper · June 2015

CITATION
1

READS
4,508

3 authors:

Madhu Kodati
Indian Institute of Technology Madras
3 PUBLICATIONS **19** CITATIONS
SEE PROFILE

Vikranth Reddy
Indian Institute of Technology Madras
4 PUBLICATIONS **33** CITATIONS
SEE PROFILE

Sandipan Bandyopadhyay
Indian Institute of Technology Madras
107 PUBLICATIONS **558** CITATIONS
SEE PROFILE

Kinematic analysis of MacPherson strut suspension system

Madhu Kodati* K. Vikranth Reddy† Sandipan Bandyopadhyay‡
IIT Madras IIT Madras IIT Madras
Chennai, India Chennai, India Chennai, India

Abstract—*The MacPherson strut (MPS) suspension system is one of the most common independent automobile suspensions. This paper presents a kinematic analysis for the complete spatial model of the same. The presented solution is built upon two key elements in the formulation and solution stages, respectively: use of Rodrigue's parameters to develop an algebraic set of equations representing the kinematics, and computation of Gröbner basis as a method of solving the resulting set of polynomial equations. It is found that the final univariate equation representing all the kinematic solutions for a given pair of steering and road profile inputs is of 64 degree - which reflects the complexity observed in the kinematics of the mechanism. The real roots of this polynomial are extracted with high numerical precision and are validated. Finally, they are used to find the configuration of the mechanism for a particular set of road and steering inputs.*

Keywords: MacPherson strut, Spatial kinematics, Polynomial equations, Gröbner basis, Rodrigue's parameters

I. Introduction

MacPherson strut suspensions are among the simplest and most commonly used suspension systems globally, in passenger cars. American automotive engineer Earle S. MacPherson developed the MPS using a strut configuration [1]. Solid model of the suspension system is shown in Fig. 1. One end of the strut is attached to the knuckle with a prismatic joint and other end is fixed to the chassis by a spherical joint. The strut also contains the spring and damping elements. The lower arm is connected to chassis by a revolute joint, and the other end is connected to the knuckle by a spherical joint. The steering link is attached to the tie-rod using spherical joints and the tie-rod is connected to the rack with a universal joint. Though the MPS has less favourable kinematic characteristics compared to a double wish-bone suspension [2], it is compact enough to be compatible with the transversely mounted engines, and is thus used widely for front-wheel-drive cars.

Numerous techniques for the kinematic analysis of MPS suspension exist in literature, a prominent one being [1]. Modelling the MPS as a spatial mechanism, linear and non-linear position analysis was done based on vector algebra.

*madhukodati@gmail.com
†vikranthiit@gmail.com
‡sandipan@iitm.ac.in

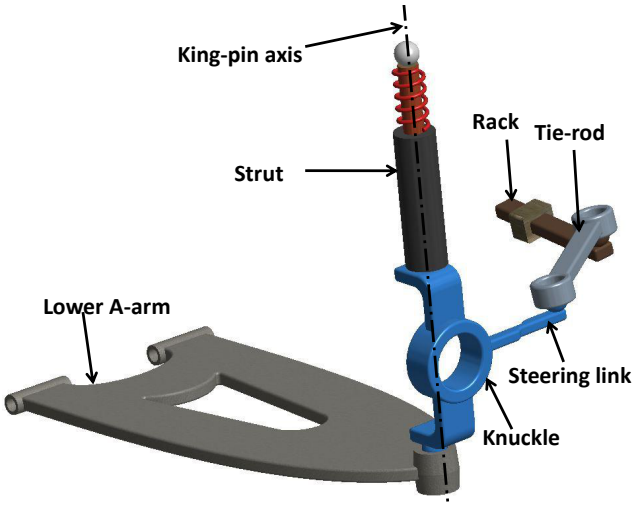

Fig. 1. Simplified solid model of the MacPherson strut

Later, H.A. Attia [3] presented a formulation in terms of Cartesian coordinates of some defined points in the links and at the kinematic joints, whereas, D.A. Mántaras et al. [4] formed the constraint equations using Euler parameters.

The above methodologies implemented the Newton-Raphson method subsequently to solve the non-linear equations for the unknown variables. However, it is well-known that this method has issues regarding not converging to a solution in the absence of a "good" initial guess solution and its inability to capture all the possible solutions. Addressing this, Y.A. Papegay et al. [5] tried to solve the MPS suspension kinematics problem using symbolic computation techniques. However, exact solution in symbolic form by employing Gröbner basis on constraint equations was reported to be unachievable.

The design of the MPS involves a relatively large number of elements, and thus has a reasonably large design space. This affords better control over the kinematic response of the suspension. However, for the same reason, a significant difficulty presents itself in any kinematic/dynamic study of such systems: the complexity of their kinematics. As a mechanism, the MPS possesses two degrees-of-freedom: one accounting for the steering input $s(t)$, and the other accommodating jounce and rebound, the road profile input $y(t)$[1].

[1]The steering input and road profile input are denoted henceforth by s

Finding the output or response of the MPS to these inputs, e.g., determining the location and orientation of the kingpin axis (KPA) for a combination of s and y, which is important for understanding the ride and handling characteristics, driving behaviour [2], is a formidable task. Once found, these kinematic solutions give greater accuracy when used to study different design configurations, and optimization of the architecture parameters of the suspension mechanism with performance indices like camber, caster and toe as objectives.

This paper presents a kinematic model and analysis of the MPS suspension which follows a similar treatment of the double-wishbone suspension system presented in [6]. The kinematic equations of the MPS are formulated in an algebraic manner by representing the orientation of the KPA in terms of Rodrigue's parameters $\boldsymbol{c} = (c_1, c_2, c_3)^\top$ (see e.g., [7]). Retaining the symbolic form of these equations and eliminating the unknowns which occur as linear terms, leads to a system of three quartic equations in the three Rodrigue's parameters. Attempts to reduce this system of equations in symbolic form to an univariate of degree 64 in one of the three parameters (c_1, c_2, c_3), were unsuccessful. The equations are therefore solved by substituting the numerical values for the architecture parameters of the MPS along with the inputs s and y. The solution technique involves finding the Gröbner basis of the ideal generated by the three equations and extracting the roots of final univariate with a high numerical precision. The real roots of the polynomials are used to completely determine the configuration of the suspension. The obtained results are validated numerically to ascertain the correctness of the proposed method.

The rest of the paper is organised as follows: In Section II, formulation of the loop-closure equations, elimination of the variables for two possible cases and methodology for finding solutions are presented. Finally, the configurations of the suspension for real solutions of the loop-closure equations are depicted graphically. In Section III, the conclusions are presented.

II. Kinematic analysis of MacPherson strut suspension

The eventual success in solving any position kinematics problem relies upon an appropriate kinematic modelling, efficient formulation, as well as effective solution techniques. The details of these, as applied to the present problem, are presented in this section under the following modelling assumptions:

- The cushioning effect of the bushes at the joints are not considered, i.e., only ideal joints are considered in the formulation.
- The flexibility of the links are not considered, only rigid links are used in the formulation.

and y respectively, by dropping the explicit time dependence.

- The chassis is considered to be the *fixed* or the *ground* link in the mechanism.
- All the geometric parameters of the suspension mechanism are exactly known.
- The universal joint between the tie-rod and the rack is replaced with a kinematically equivalent spherical joint.

A. Geometry of the MPS

The schematic of the MPS suspension is shown in Fig. 2. Kinematically, it is a combination of a spatial four-bar loop $\boldsymbol{o}_0\boldsymbol{p}_1\boldsymbol{o}_1\boldsymbol{o}_0$ (which is an inverted slider mechanism that has chassis as the ground link and king-pin as the coupler), and a spatial five-bar loop $\boldsymbol{o}_0\boldsymbol{p}_1\boldsymbol{p}_3\boldsymbol{p}_4\boldsymbol{p}_8\boldsymbol{o}_0$. These two loops are coupled at the king-pin (link ② in Fig. 2).

Two coordinate systems are used to describe the configuration of the MPS. The global frame of reference $\{0\}$ is attached to $\boldsymbol{o}_0$, and its Z_0-axis is aligned to the axis of the hinges of the lower A-arm. The lower A-arm is equivalently represented as a single link (link ① in Fig. 2) which moves in the X_0Y_0-plane. The prismatic pair between $\boldsymbol{p}_1$ and $\boldsymbol{o}_1$ is considered to be a single link of variable length l_2. A body-fixed frame of reference, $\{1\}$, is attached to $\boldsymbol{p}_1$. The X-axis of $\{1\}$ (denoted by X_1) is along the link vector $\boldsymbol{l}_2 = \boldsymbol{o}_1 - \boldsymbol{p}_1$, and X_1Y_1-plane contains link ③.

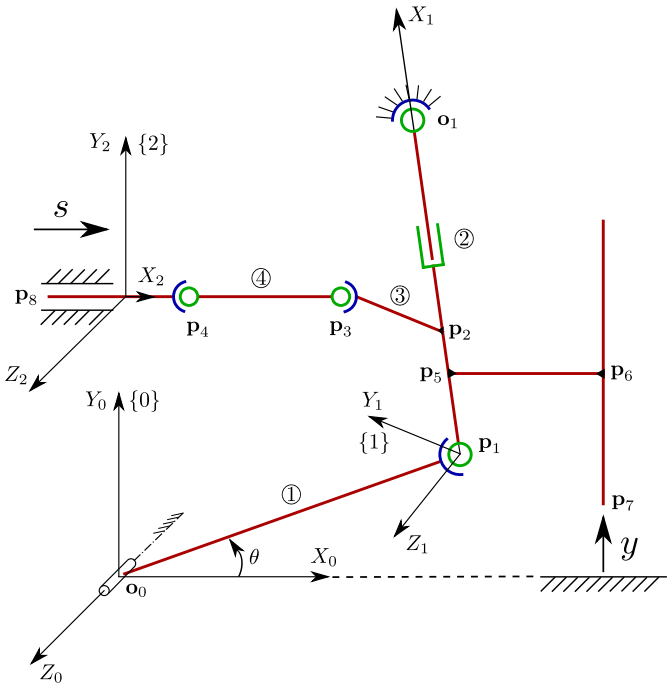

Fig. 2. Schematic of the MacPherson strut suspension mechanism

Any vector in the body-fixed frame of reference can be *transformed* to the global frame of reference by pre-multiplying with an appropriate rotation matrix $\boldsymbol{R} \in SO(3)$ (see, e.g., [8]). The rotation matrix ${}^0_1\boldsymbol{R}$ relates the orientation of $\{1\}$ w.r.t. $\{0\}$ i.e., the orientation of KPA w.r.t. the global frame of reference. In the presented for-

mulation, it is expressed in terms of the Rodrigue's parameters, $\boldsymbol{c} = (c_1, c_2, c_3)^\top \in \mathbf{R}^3$. This is a key step in the kinematic modelling, as this parametrisation leads to an *algebraic* description of the orientation of the KPA, which in turn, helps in formulating the *loop-closure* equations in algebraic terms, as explained in the next subsection.

B. Formulation of the loop-closure equations

For brevity, all vectors expressed in the global frame of reference $\{0\}$ are written henceforth without the leading super-script '0'; e.g., as $\boldsymbol{p}$, $\boldsymbol{l}$ instead of ${}^0\boldsymbol{p}$, ${}^0\boldsymbol{l}$ respectively. The rack/steering input, s, is given at the point $\boldsymbol{p}_8$, and the road profile input, y, is applied to the point $\boldsymbol{p}_7$ (see Fig. 2). The end points of link ② can be expressed as:

$$\boldsymbol{p}_1 = \boldsymbol{o}_0 + \boldsymbol{R}_{Z_0}(\theta)[l_1, 0, 0]^\top, \text{ and} \tag{1}$$

$$\boldsymbol{o}_1 = [o_{1x}, o_{1y}, o_{1z}]^\top, \tag{2}$$

respectively. The vector $\boldsymbol{l}_2$ can be expressed as:

$$\boldsymbol{l}_2 = \boldsymbol{o}_1 - \boldsymbol{p}_1, \text{ or} \tag{3}$$

$$\boldsymbol{l}_2 = {}^0_1\boldsymbol{R}[l_2, 0, 0]^\top. \tag{4}$$

From Eqs. (1-4), one can write:

$$\boldsymbol{o}_1 - \boldsymbol{o}_0 - \boldsymbol{R}_{Z_0}(\theta)[l_1, 0, 0]^\top - {}^0_1\boldsymbol{R}[l_2, 0, 0]^\top = \mathbf{0}. \tag{5}$$

Eq. (5) models the kinematics of the four-bar loop $\boldsymbol{o}_0\boldsymbol{p}_1\boldsymbol{o}_1\boldsymbol{o}_0$. The expression on the left hand side of Eq. (5) is of the form:

$$\boldsymbol{\eta}_1 = (\eta_{1x}, \eta_{1y}, \eta_{1z})^\top, \tag{6}$$

where η_{1x}, η_{1y} and η_{1z} are given by:

$$\eta_{1x} = -l_2\left(c_1^2 - c_2^2 - c_3^2 + 1\right) - c_\Delta l_1 \cos\theta + c_\Delta o_{1x}, \tag{7}$$

$$\eta_{1y} = -2l_2(c_1c_2 + c_3) - c_\Delta l_1 \sin\theta + c_\Delta o_{1y}, \tag{8}$$

$$\eta_{1z} = -2l_2(c_1c_3 - c_2) + c_\Delta o_{1z}, \text{ where} \tag{9}$$

$$c_\Delta = 1 + c_1^2 + c_2^2 + c_3^2. \tag{10}$$

The end points of link ④ can be expressed as:

$$\boldsymbol{p}_3 = \boldsymbol{p}_1 + {}^0_1\boldsymbol{R}^1\boldsymbol{l}_3, \text{ and} \tag{11}$$

$$\boldsymbol{p}_4 = [p_{4x} + s_x, p_{4y} + s_y, p_{4z} + s_z]^\top, \tag{12}$$

where ${}^1\boldsymbol{l}_3 = (l_{3x}, l_{3y}, l_{3z})^\top$ is the vector from $\boldsymbol{p}_1$ to ${}^1\boldsymbol{p}_3$ (expressed in $\{1\}$) and $\boldsymbol{s} = (s_x, s_y, s_z)^\top$ is the rack input vector in $\{0\}$, given by:

$$\boldsymbol{s} = {}^0_2\boldsymbol{R}[s, 0, 0]^\top, \text{ where}$$
$${}^0_2\boldsymbol{R} = \boldsymbol{R}_Z(\beta_1)\boldsymbol{R}_Y(\beta_2)\boldsymbol{R}_X(\beta_3).$$

The vector $\boldsymbol{l}_4$ can be expressed as:

$$\boldsymbol{l}_4 = \boldsymbol{p}_4 - \boldsymbol{p}_3.$$

The loop-closure constraints of the five-bar loop $\boldsymbol{o}_0\boldsymbol{p}_1\boldsymbol{p}_3\boldsymbol{p}_4\boldsymbol{p}_8\boldsymbol{o}_0$ can be reduced to the following equation:

$$(\boldsymbol{p}_4 - \boldsymbol{p}_3) \cdot (\boldsymbol{p}_4 - \boldsymbol{p}_3) - l_4^2 = 0. \tag{13}$$

The expression on the left hand side of Eq. (13) is denoted by η_2. From the road input to the lower A-arm loop, $\boldsymbol{o}_0\boldsymbol{p}_1\boldsymbol{p}_5\boldsymbol{p}_7\boldsymbol{o}_0$, one can write:

$$[p_{7x} + x, p_{7y} + y, p_{7z} + z]^\top - {}^0_1\boldsymbol{R}^1\boldsymbol{l}_5$$
$$-{}^0_1\boldsymbol{R}[r_2, 0, 0]^\top - \boldsymbol{R}_{Z_0}(\theta)[l_1, 0, 0]^\top - \boldsymbol{o}_0 = \mathbf{0}, \tag{14}$$

where x, z are lateral and longitudinal displacements of $\boldsymbol{p}_7$ w.r.t global frame of reference, which vary upon changing s and y; ${}^1\boldsymbol{l}_5 = (l_{5x}, l_{5y}, l_{5z})^\top$ is the vector from ${}^1\boldsymbol{p}_5$ to ${}^1\boldsymbol{p}_7$ (expressed in $\{1\}$). The parameter r_2 is the distance between $\boldsymbol{p}_1$ and $\boldsymbol{p}_5$. The expression on the left hand side of Eq. (14) is of the form:

$$\boldsymbol{\eta}_3 = (\eta_{3x}, \eta_{3y}, \eta_{3z})^\top, \tag{15}$$

where η_{3x}, η_{3y} and η_{3z} are given by:

$$\begin{aligned}\eta_{3x} =& -l_{5x}\left(c_1^2 - c_2^2 - c_3^2 + 1\right) - 2l_{5y}(c_1c_2 - c_3)\\ &- 2l_{5z}(c_1c_3 + c_2) - r_2\left(c_1^2 - c_2^2 - c_3^2 + 1\right) - c_\Delta l_1\cos\theta\\ &+ c_\Delta p_{7x} + c_\Delta x,\end{aligned} \tag{16}$$

$$\begin{aligned}\eta_{3y} =& -2l_{5x}(c_1c_2 + c_3) - l_{5y}\left(-c_1^2 + c_2^2 - c_3^2 + 1\right)\\ &- 2l_{5z}(c_2c_3 - c_1) - 2r_2(c_1c_2 + c_3) - c_\Delta l_1\sin\theta\\ &+ c_\Delta p_{7y} + c_\Delta y,\end{aligned} \tag{17}$$

$$\begin{aligned}\eta_{3z} =& -l_{5z}\left(-c_1^2 - c_2^2 + c_3^2 + 1\right) - 2l_{5x}(c_1c_3 - c_2)\\ &- 2l_{5y}(c_1 + c_2c_3) - 2r_2(c_1c_3 - c_2) + c_\Delta p_{7z} + c_\Delta z.\end{aligned} \tag{18}$$

Eqs. (7-9), Eq. (13) and Eqs. (16-18) together define the kinematics of the MPS suspension system.

TABLE I. Structure of the loop-closure constraints of the MPS suspension mechanism

Equation	LHS	Variables	Size (KB)
Eq. (7)	η_{1x}	$c_1, c_2, c_3, l_2, \cos\theta$	1.031
Eq. (8)	η_{1y}	$c_1, c_2, c_3, l_2, \sin\theta$	0.703
Eq. (9)	η_{1z}	c_2, c_1, c_3, l_2	0.687
Eq. (13)	η_2	$c_1, c_2, c_3, \cos\theta, \sin\theta$	15.937
Eq. (16)	η_{3x}	$c_1, c_2, c_3, x, \cos\theta$	3.148
Eq. (17)	η_{3y}	$c_1, c_2, c_3, \sin\theta$	2.820
Eq. (18)	η_{3z}	c_1, c_2, c_3, z	2.805

C. Elimination of variables

The variables included in, and the *sizes*[2] of the equations obtained in the Section II-B are summarised in the Table I.

[2] All the symbolic computations have been performed using the commercial computer algebra software, Mathematica [9]. The "size", in this context, refers to the amount of *computer memory* needed to represent/store an expression in Mathematica's internal format.

The sequence of elimination of variables needs to be chosen so as to reduce the complexity of the resulting equations. To begin with, it is to be noted that the loop-closure equations are *linear* in terms of sine and cosines of the angle θ and in l_2. Discussed below are the two possible cases of kinematic solutions.

C.1 Case-1: $(c_2 - c_1 c_3) \neq 0$

The above-mentioned variables are eliminated in a sequential manner, as shown schematically in Fig. 3.

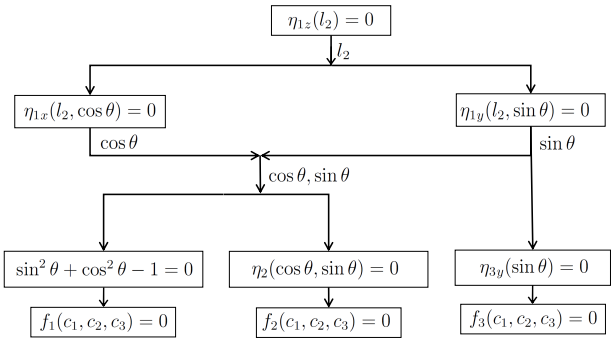

Fig. 3. Sequence of elimination of $\cos\theta, \sin\theta$ and l_2 from Eq. (7-9), Eq. (13) & Eq. (17) for Case-1

First, l_2 is computed from Eq. (9) and substituted in Eq. (7) and Eq. (8). The functions η_{1x} and η_{1y} are linear in terms of $\cos\theta$ and $\sin\theta$. Hence Eq. (7) and Eq. (8) are solved simultaneously to obtain $\cos\theta$ and $\sin\theta$, respectively. The eliminated variables, l_2, $\cos\theta$ and $\sin\theta$ are found to be:

$$l_2 = \frac{-c_\Delta o_{1z}}{2\,(c_2 - c_1 c_3)}, \tag{19}$$

$$\cos\theta = \frac{-2c_3 c_1 o_{1x} + 2c_2 o_{1x} + c_1^2 o_{1z} - c_2^2 o_{1z} - c_3^2 o_{1z} + o_{1z}}{2\,(c_2 - c_1 c_3)\,l_1}, \tag{20}$$

$$\sin\theta = \frac{c_2 o_{1y} - c_1 c_3 o_{1y} + c_1 c_2 o_{1z} + c_3 o_{1z}}{(c_2 - c_1 c_3)\,l_1}. \tag{21}$$

It is to be noted that the denominators in the expressions for l_2, $\cos\theta$ and $\sin\theta$ do not vanish as per the stated assumption. The variable θ is eliminated using the identity $\sin^2\theta + \cos^2\theta - 1 = 0$, which gives rise to the equation $f_1(c_1, c_2, c_3) = 0$. Note that f_1 is free of any other unknowns than those mentioned explicitly. Similarly, the expressions for $\sin\theta$ and $\cos\theta$ are substituted in Eq. (13), which leads to the equation $f_2(c_1, c_2, c_3) = 0$. Finally, The expression for $\sin\theta$ is substituted in Eq. (17), to obtain the equation $f_3(c_1, c_2, c_3) = 0$.

The functions f_1, f_2, f_3 form a system of three quartic equations in the unknowns c_1, c_2, c_3. They may be written compactly as:

$$f_1(c_1, c_2, c_3) = \sum_{i=0}^{4}\sum_{j=0}^{4}\sum_{k=0}^{4} u_{ijk} c_1^i c_2^j c_3^k, \tag{22}$$

$$f_2(c_1, c_2, c_3) = \sum_{i=0}^{4}\sum_{j=0}^{4}\sum_{k=0}^{4} v_{ijk} c_1^i c_2^j c_3^k, \tag{23}$$

$$f_3(c_1, c_2, c_3) = \sum_{i=0}^{4}\sum_{j=0}^{4}\sum_{k=0}^{4} w_{ijk} c_1^i c_2^j c_3^k; \tag{24}$$

$$i + j + k \leq 4.$$

The coefficients u_{ijk}, v_{ijk}, and w_{ijk} in Eqs. (22-24) are functions of the architecture parameters of the MPS. These are obtained symbolically using `Mathematica`[3], and simplified to their *monomial-based canonical forms* [10]. The sizes of the polynomials after simplification are 5.961 KB, 32.672 KB, and 5.844 KB respectively.

C.2 Case-2: $(c_2 - c_1 c_3) = 0$

In this case, Eq. (9) becomes

$$o_{1z} = 0, \quad \text{as } c_\Delta \neq 0, \tag{25}$$

which is physically admissible. The variables l_2, $\sin\theta$ and $\cos\theta$ are eliminated in a different manner in this case, which is shown schematically in Fig. (4).

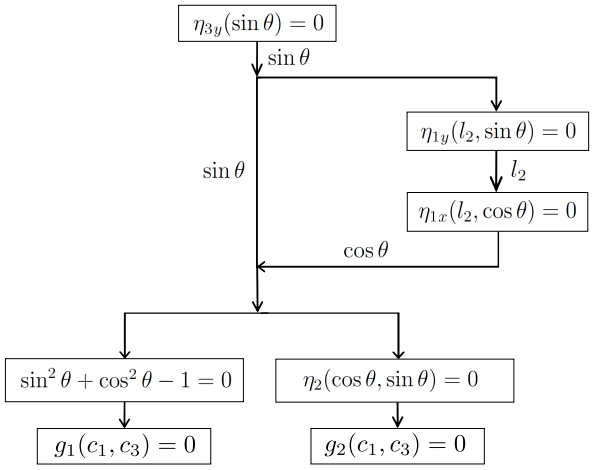

Fig. 4. Sequence of elimination of $\cos\theta, \sin\theta$ and l_2 from Eq. (7, 8), Eq. (13) & Eq. (17) for Case-2

The functions g_1, g_2 form a system of equations in the

[3]All the computations in this paper were done in Mathematica version-9.0.0 for 64-bit Linux O.S. on a system with 6-core Intel Core i7-4930K CPU @ 3.40 GHz clock speed and 64 GB of RAM.

unknowns c_1, c_3 and are written compactly as:

$$g_1(c_1, c_3) = \sum_{i=0}^{4} \sum_{j=0}^{6} m_{ij} c_1^i c_3^j, \tag{26}$$

$$g_2(c_1, c_3) = \sum_{i=0}^{2} \sum_{j=0}^{4} n_{ij} c_1^i c_3^j. \tag{27}$$

The coefficients m_{ij}, n_{ij} in Eqs. (26, 27) are again functions of the architecture parameters of the MPS. These coefficients are obtained symbolically using `Mathematica`, and are simplified to their monomial-based canonical forms. The sizes of the polynomials after simplification are 24.305 KB and 19.305 KB respectively.

D. Solutions for system of quartic equations

D.1 Case-1: $(c_2 - c_1 c_3) \neq 0$

It would be ideal indeed to solve Eqs. (22-24) for the most general case, i.e., keeping all of the coefficients in their symbolic forms. However, attempts to eliminate two of the three remaining variables to obtain a *univariate* in the third variable in terms of *symbolic* coefficients did not succeed. Hence these equations are solved for given numerical instances of design parameters (given in Table II), and inputs (s, y). The solution procedure used, however,

TABLE II. Architecture parameter values of the MPS (base data is taken from [1] and transformed to match the given reference frame)

Parameter	**Symbol**	**Value**[4]
Length of lower A-arm	l_1	0.322
Length of tie rod	l_4	0.361
Link-3 vector w.r.t. {1}	(l_{3x}, l_{3y}, l_{3z})	(0.106, 0.108, 0)
Position of origin of {0}	$\boldsymbol{o}_0$	(0, 0, 0)
Position of strut mounting	$\boldsymbol{o}_1$	(0.136, 0.497, 0.011)
Initial position of $\boldsymbol{p}_4$	(p_{4x}, p_{4y}, p_{4z})	(-0.078, 0.105, -0.108)
Euler angles relating {2} to {0}	$(\beta_1, \beta_2, \beta_3)$	(-1.534, 0.019, 0.072)
Initial position of $\boldsymbol{p}_7$	(p_{7x}, p_{7y}, p_{7z})	(0.434, -0.333, -0.019)
Link-5 vector w.r.t. {1}	(l_{5x}, l_{5y}, l_{5z})	(-0.505, 0.009, 0.054)
Distance between $\boldsymbol{p}_1$ and $\boldsymbol{p}_2$	r_1	0.106
Distance between $\boldsymbol{p}_1$ and $\boldsymbol{p}_5$	r_2	0.061

is *semi-analytical* in nature, and involves the computation of the *Gröbner basis* (see, e.g., [11]) generated by the *ideal* $\mathcal{F} = \langle f_1, f_2, f_3 \rangle$. This prevents the *degree-explosion*, which happens otherwise, if pair-wise resultants are computed. The details of this final stage of elimination and solution are presented in the rest of this section. The sample inputs considered for all numerical computations to explain the methodology are $s = 50$mm and $y = 50$mm.

After substitution of the numerical values as per the Table II, the coefficients u_{ijk}, v_{ijk}, and w_{ijk} in Eqs. (22-24) are found in their numerical forms with default `MachinePrecision` in `Mathematica`. The *ideal* $\mathcal{F}$ is defined in `SINGULAR` [12] under a ring of real coefficients with a numerical precision of 200 and lexicographical monomial ordering on c_1, c_2, c_3, i.e., $c_1 \succ c_2 \succ c_3$. The Gröbner basis of $\mathcal{F}$ consists of three polynomials: $h_1(c_3)$, $h_2(c_2, c_3)$, and $h_3(c_1, c_3)$. Among these, h_1 is a univariate polynomial in c_3 of degree 64:

$$h_1 = a_0 c_3^{64} + a_1 c_3^{63} + \cdots + a_{64} = 0. \tag{28}$$

Each of a_is in Eq. (28) are floating-point numbers with 200 significant digits. The polynomials h_2, h_3 are *linear* in c_2 and c_1 respectively, and of degree 63 in c_3.

Extraction of the real roots of the polynomial h_1 using the `SINGULAR` routine `laguerre_solve` (for which, the internal computation precision as well as the output precision is again set to 200) yields $c_3 = 1.436, 1.556$. These real solutions for c_3 are substituted back in h_2 and h_3 to obtain the corresponding real solutions for c_2 and c_1: (c_1, c_2)= (-1.678, -2.599) and (0.879, 1.289).

The solutions of c_1, c_2 and c_3 obtained above are back-substituted in Eqs. (7-9) and Eqs. (16-18) to compute the corresponding solutions for θ, l_2, x and z which are given in Table III.

TABLE III. Values of θ, x and z for $s = 50$mm, $y = 50$mm for Case-1

(c_1, c_2, c_3)	θ(rad)	x(mm)	z(mm)	l_2(mm)
(-1.678, -2.599, 1.436)	0.451	-6.517	-30.094	367.407
(0.879, 1.289, 1.556)	0.332	94.594	26.519	403.550

The configurations of the mechanism for real solutions of c_1, c_2 and c_3 for various inputs are depicted in Figs. 5 - 8, and the residual values of initial loop-closure equations are listed in the Table IV, which establish the numerical accuracy of the solutions obtained.

D.2 Case-2: $(c_2 - c_1 c_3) = 0$

Eq. (26) and Eq. (27) are solved following the same procedure i.e., by defining the ideal $\mathcal{G} = \langle g_1, g_2 \rangle$ and finding the Gröbner basis of $\mathcal{G}$, which consists of two polynomials: $t_1(c_3)$ and $t_2(c_1, c_3)$. Among these, t_1 is a univariate polynomial in c_3 of degree 28:

$$t_1 = b_0 c_3^{28} + b_1 c_3^{27} + \cdots + b_{28} = 0. \tag{29}$$

Each of b_is in Eq. (29) are floating-point numbers with 200 significant digits. The polynomial t_2 is *linear* in c_1 and of degree 27 in c_3.

TABLE IV. Residuals of Eq. (5), Eq. (13) and Eq. (14) for Case - 1

S.No	s(mm)	y(mm)	(c_1, c_2, c_3)	**Residuals** $\times 10^{-11}$		
				$\|\boldsymbol{\eta}_1\|$	$\|\eta_2\|$	$\|\boldsymbol{\eta}_3\|$
1	0	-100	(-0.958, -1.417, 1.411)	4.360	330.553	0.017
			(0.491, 0.663, 1.430)	2.933	121.879	0.131
2	50	50	(-1.678, -2.599, 1.436)	1.694	116.129	0.716
			(0.879, 1.289, 1.556)	2.676	202.719	0.969
3	0	60	(-1.044, -1.632, 1.459)	2.063	152.210	0.978
			(0.595, 0.858, 1.548)	1.894	101.232	0.767
4	50	-100	(-1.615, -2.358, 1.385)	3.477	245.735	0.205
			(0.772, 1.057, 1.434)	4.563	314.927	0.460

[4]Positions, lengths are given in metres and angles are given in radians.

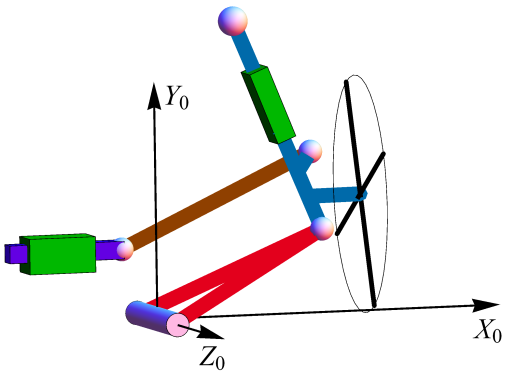

(a) $\boldsymbol{c} = (-1.678, -2.599, 1.436)^\top$

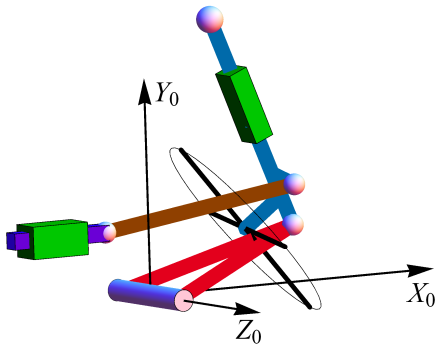

(b) $\boldsymbol{c} = (0.879, 1.289, 1.556)^\top$

Fig. 5. Configurations corresponding to the real values of c_1, c_2, c_3 for $s = 50$mm, $y = 50$mm for Case-1

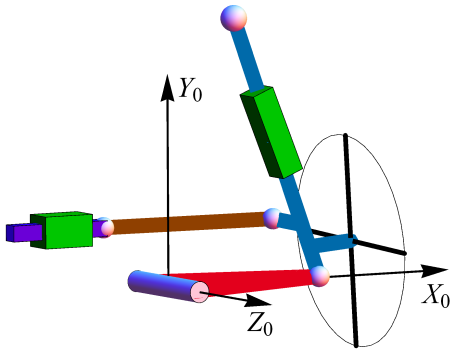

(a) $\boldsymbol{c} = (-0.958, -1.417, 1.411)^\top$

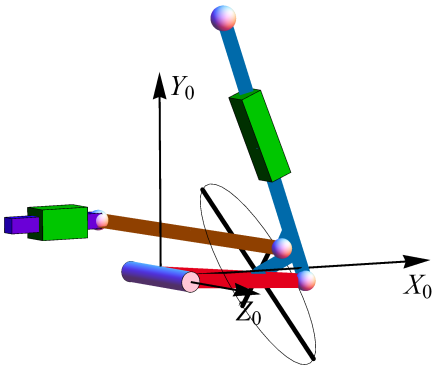

(b) $\boldsymbol{c} = (0.491, 0.663, 1.430)^\top$

Fig. 6. Configurations corresponding to the real values of c_1, c_2, c_3 for $s = 0$mm, $y = -100$mm for Case-1

Extraction of the real roots of the polynomial t_1 in SINGULAR yields $c_3 = 1.518, 1.520$. These real solutions for c_3 are substituted back in t_2 to obtain corresponding real solutions for c_1 as $0.861, -1.774$. Finally, the corresponding values for c_2 are obtained using $c_2 = c_1 c_3$ as $1.307, -2.696$ respectively.

The values of c_1, c_2 and c_3 are back-substituted in Eqs. (7-8) and Eqs. (16-18) to compute the corresponding solutions for θ, l_2, x and z which are given in Table V.

TABLE V. Values of θ, x and z for $s = 50$mm, $y = 50$mm for Case-2

(c_1, c_2, c_3)	θ(rad)	x(mm)	z(mm)	l_2(mm)
(0.861, 1.307, 1.518)	0.330	94.924	37.558	427.958
(-1.774, -2.696, 1.520)	0.455	-6.553	-16.923	387.864

The configurations of the mechanism for real solutions of c_1, c_2 and c_3 for various inputs are depicted in Fig. 9-12, and the residual values of initial loop-closure equations are listed in the Table VI.

TABLE VI. Residuals of Eq. (5), Eq. (13) and Eq. (14) for Case - 2

S.No	s(mm)	y(mm)	(c_1, c_2, c_3)	**Residuals** $\times 10^{-13}$		
				$\|\boldsymbol{\eta}_1\|$	$\|\eta_2\|$	$\|\boldsymbol{\eta}_3\|$
1	0	-100	(0.484, 0.684, 1.414)	1.172	157.230	0.568
			(-0.981, -1.417, 1.444)	1.271	1345.500	0.568
2	50	50	(0.861, 1.307, 1.518)	0.568	202.367	0.036
			(-1.774, -2.696, 1.520)	0.636	339.277	0.568
3	0	60	(-1.097, -1.661, 1.514)	0.568	1444.240	0.568
			(0.577, 0.878, 1.521)	0.568	527.021	0.568
4	50	-100	(0.767, 1.081, 1.410)	1.137	368.108	0.604
			(-1.662, -2.394, 1.441)	1.271	402.446	0.568

III. Conclusions

This paper presents a complete study of the position kinematics of the MacPherson suspension system with the formulation based on algebraic parametrisation of the orientation of the KPA. Two elimination schemes are presented based on the relationship between the orientation parameters, following which, the initial set of five simultaneous algebraic-trigonometric loop-closure equations reduces to system of three and two polynomial equations. These two sets of polynomials are solved separately by finding

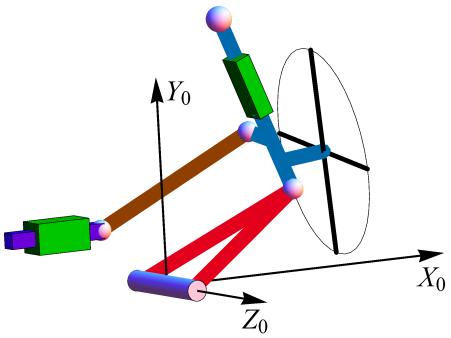

(a) $\boldsymbol{c} = (-1.044, -1.632, 1.459)^\top$

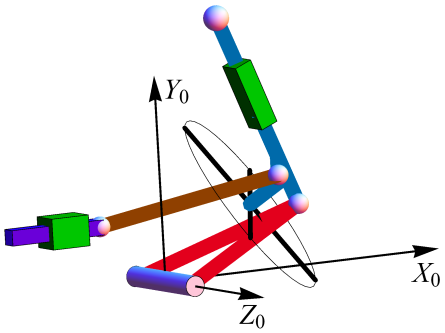

(b) $\boldsymbol{c} = (0.595, 0.858, 1.548)^\top$

Fig. 7. Configurations corresponding to the real values of c_1, c_2, c_3 for $s = 0$mm, $y = 60$mm for Case-1

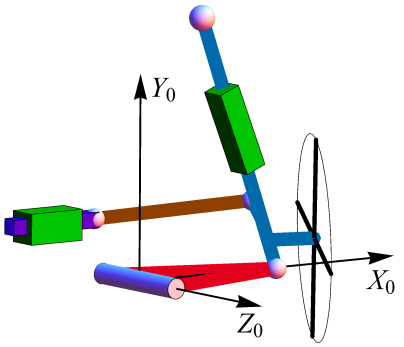

(a) $\boldsymbol{c} = (-1.615, -2.358, 1.385)^\top$

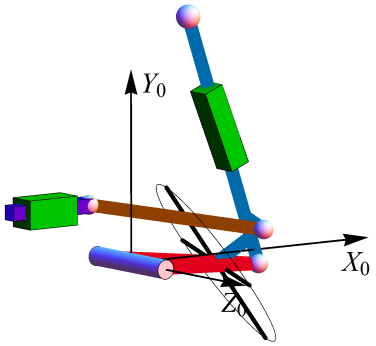

(b) $\boldsymbol{c} = (0.772, 1.057, 1.434)^\top$

Fig. 8. Configurations corresponding to the real values of c_1, c_2, c_3 for $s = 50$mm, $y = -100$mm for Case-1

Gröbner basis of the ideal formed by the respective set after substituting numerical values for the architecture parameters and inputs. The methodology developed is semi-analytical in nature, as the loop-closure constraints are reduced to three polynomials retaining the geometric parameters and inputs in their symbolic form. The final univariate polynomial in one of the parameters of interest turns out to be of degree 64 and of 28 for the respective cases. Real solutions with high numerical precision are extracted and are validated by computing the residuals of the initial set of equations. Possible configurations of the MPS for all real solutions obtained for various combinations of inputs are depicted graphically. Out of 64 and 28 possible number of solutions in the two possible cases, two solutions turn out to be real and only one of them corresponds to a physically feasible configuration of the MPS. While this is observed consistently in all the numerical examples reported here, the number of real solutions in the generic case is yet to be studied.

The main contribution of the paper is to present a methodology for finding solution of the MPS suspension position analysis problem in its full complexity. The motivation behind this paper is to support and develop a formulation technique for detailed analysis/optimisation of the MPS design, as well the study of its dynamics. It is to be noted that the entire formulation, which contains symbolic computations and numerical solution finding techniques with high precision takes around 0.6 seconds[5] to arrive at the possible configurations of the mechanism for a given set of input values. Future work would focus on finding the final resultant/univariate of the loop-closure equations purely in symbolic form.

IV. Appendices

A. *Rodrigue's parameters*

Rodrigue's parameters provide an algebraic parametrisation of $SO(3)$. The rotation matrix ${}^0_1\boldsymbol{R}$ in terms of the three

[5]On a system with 64-bit Linux O.S. and 6-core Intel Core i7-4930K CPU @ 3.40 GHz clock speed and 64 GB of RAM.

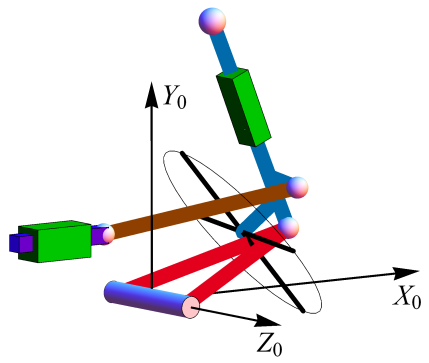

(a) $\boldsymbol{c} = (0.861, 1.307, 1.518)^\top$

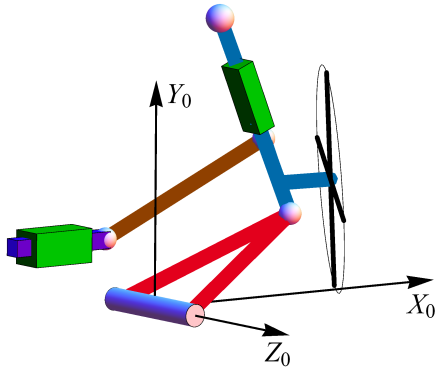

(b) $\boldsymbol{c} = (-1.774, -2.696, 1.520)^\top$

Fig. 9. Configurations corresponding to the real values of c_1, c_2, c_3 for $s = 50$mm, $y = 50$mm for Case-2

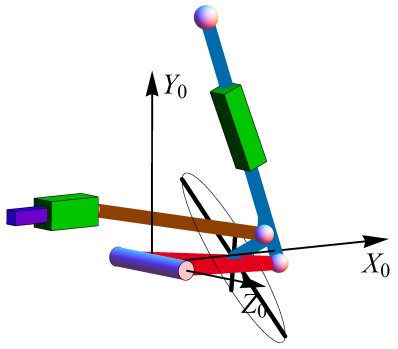

(a) $\boldsymbol{c} = (0.484, 0.684, 1.414)^\top$

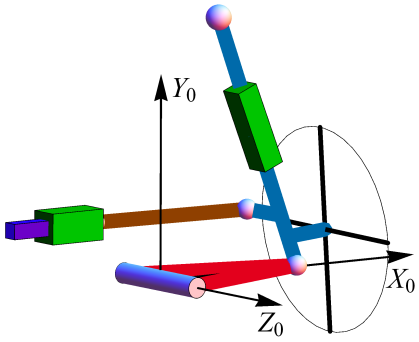

(b) $\boldsymbol{c} = (-0.981, -1.417, 1.444)^\top$

Fig. 10. Configurations corresponding to the real values of c_1, c_2, c_3 for $s = 0$mm, $y = -100$mm for Case-2

Rodrigue's parameters (c_1, c_2, c_3) is given by:

$$ {}^0_1\boldsymbol{R} = \frac{1}{c_\Delta}\begin{pmatrix} 1+c_1^2-c_2^2-c_3^2 & 2(c_1c_2-c_3) & 2(c_1c_3+c_2) \\ 2(c_1c_2+c_2) & 1-c_1^2+c_2^2-c_3^2 & 2(c_2c_3-c_1) \\ 2(c_1c_3-c_2) & 2(c_2c_3+c_2) & 1-c_1^2-c_2^2+c_3^2 \end{pmatrix} $$

where, $c_\Delta = 1 + c_1^2 + c_2^2 + c_3^2$.

B. Quartic polynomials in their symbolic form

The three quartic polynomials $f_1(c_1, c_2, c_3)$, $f_2(c_1, c_2, c_3)$, $f_3(c_1, c_2, c_3)$ in Eqs. (22-24) representing the kinematics of MPS in symbolic form are given by:

$f_1(c_1, c_2, c_3) = c_3^2c_1^2(-4l_1^2 + 4o_{1x}^2 + 4o_{1y}^2 - 2o_{1z}^2) + c_2c_3c_1(8l_1^2 - 8o_{1x}^2 - 8o_{1y}^2 + 8o_{1z}^2) + c_2^2(-4l_1^2 + 4o_{1x}^2 + 4o_{1y}^2 - 2o_{1z}^2) - 4c_3c_1^3o_{1x}o_{1z} + 4c_2c_1^2o_{1x}o_{1z} + 4c_3^3c_1o_{1x}o_{1z} + 4c_2^2c_3c_1o_{1x}o_{1z} - 4c_3c_1o_{1x}o_{1z} - 4c_2^3o_{1x}o_{1z} - 4c_2c_3^2o_{1x}o_{1z} + 4c_2o_{1x}o_{1z} - 8c_2c_3c_1^2o_{1y}o_{1z} + 8c_2^2c_1o_{1y}o_{1z} - 8c_3^2c_1o_{1y}o_{1z} + 8c_2c_3o_{1y}o_{1z} + c_1^4o_{1z}^2 + 2c_2^2c_1^2o_{1z}^2 + 2c_1^2o_{1z}^2 + c_2^4o_{1z}^2 + c_3^4o_{1z}^2 + 2c_2^2c_3^2o_{1z}^2 + 2c_3^2o_{1z}^2 + o_{1z}^2;$

$f_2(c_1, c_2, c_3) = o_{1z}(l_{3x} - p_{4x} - s_x)c_1^4 - 2c_2o_{1z}(p_{4y} + s_y)c_1^3 + c_3(-l_1^2 + l_4^2 - l_{3x}^2 - l_{3y}^2 - l_{3z}^2 - p_{4x}^2 - p_{4y}^2 - p_{4z}^2 - s_x^2 - s_y^2 - s_z^2 + 2l_{3y}o_{1y} + 2l_{3z}o_{1z} + 2o_{1x}p_{4x} - 2l_{3y}p_{4y} + 2o_{1y}p_{4y} - 2l_{3z}p_{4z} + 2o_{1x}s_x - 2p_{4x}s_x + 2l_{3x}(-o_{1x} + p_{4x} + s_x) - 2l_{3y}s_y + 2o_{1y}s_y - 2p_{4y}s_y - 2l_{3z}s_z - 2p_{4z}s_z)c_1^3 + 2c_2^2l_{3x}o_{1z}c_1^2 - 2o_{1z}(-l_{3x} + p_{4x} + s_x)c_1^2 + 4c_2c_3(l_{3y}(-o_{1x} + p_{4x} + s_x) + l_{3x}(-o_{1y} + p_{4y} + s_y))c_1^2 - 2c_3(o_{1z}(p_{4y} + s_y) + 2l_{3z}(-o_{1y} + p_{4y} + s_y) + 2l_{3y}(o_{1z} - p_{4z} - s_z))c_1^2 + c_2(l_1^2 - l_4^2 + l_{3x}^2 + l_{3y}^2 + l_{3z}^2 + p_{4x}^2 + p_{4y}^2 + p_{4z}^2 + s_x^2 + s_y^2 + s_z^2 - 2l_{3y}o_{1y} - 2l_{3z}o_{1z} - 2o_{1x}p_{4x} + 2l_{3y}p_{4y} - 2o_{1y}p_{4y} + 2l_{3z}p_{4z} + 2l_{3x}(o_{1x} - p_{4x} - s_x) - 2o_{1x}s_x + 2p_{4x}s_x + 2l_{3y}s_y - 2o_{1y}s_y + 2p_{4y}s_y + 2l_{3z}s_z + 2p_{4z}s_z)c_1^2 - 2c_3^2(2l_{3z}(o_{1x} - p_{4x} - s_x) + l_{3x}(o_{1z} - 2(p_{4z} + s_z)))c_1^2 + 4c_2^2(l_{3y}(o_{1x} - p_{4x} - s_x) + l_{3x}(o_{1y} - p_{4y} - s_y))c_1 - 2c_2^3o_{1z}(p_{4y} + s_y)c_1 + c_3^2(4l_{3y}(o_{1x} - p_{4x} - s_x) + 4l_{3x}(-o_{1y} + p_{4y} + s_y))c_1 + c_2c_3^2(4l_{3z}(-o_{1y} + p_{4y} + s_y) - 2(o_{1z}(p_{4y} + s_y) + 2l_{3y}(o_{1z} - p_{4z} - s_z)))c_1 - 8c_2c_3l_{3x}(-o_{1z} + p_{4z} + s_z)c_1 + c_2^2c_3(-l_1^2 + l_4^2 - l_{3x}^2 - l_{3y}^2 - l_{3z}^2 - p_{4x}^2 - p_{4y}^2 - p_{4z}^2 - s_x^2 - s_y^2 - s_z^2 - 2l_{3y}o_{1y} + 2l_{3z}o_{1z} + 2o_{1x}p_{4x} + 2l_{3y}p_{4y} + 2o_{1y}p_{4y} - 2l_{3z}p_{4z} + 2o_{1x}s_x - 2p_{4x}s_x - 2l_{3x}(-o_{1x} + p_{4x} + s_x) + 2l_{3y}s_y + 2o_{1y}s_y - 2p_{4y}s_y - 2l_{3z}s_z - 2p_{4z}s_z)c_1 + c_3^3(-l_1^2 + l_4^2 - l_{3x}^2 - l_{3y}^2 - l_{3z}^2 - p_{4x}^2 -$

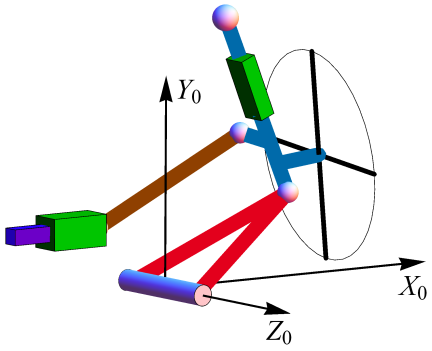

(a) $\boldsymbol{c} = (-1.097, -1.661, 1.514)^\top$

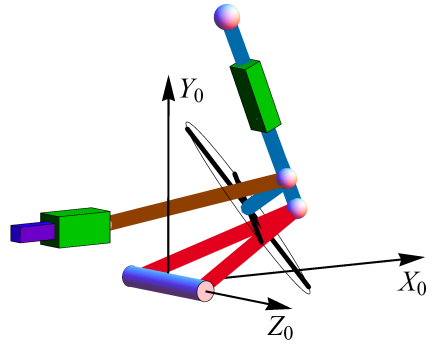

(b) $\boldsymbol{c} = (0.577, 0.878, 1.521)^\top$

Fig. 11. Configurations corresponding to the real values of c_1, c_2, c_3 for $s = 0$mm, $y = 60$mm for Case-2

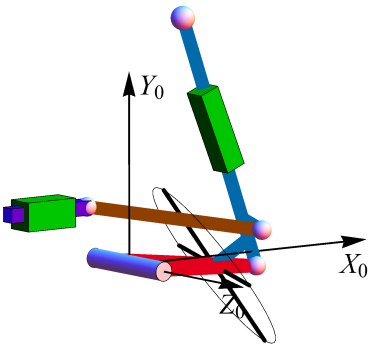

(a) $\boldsymbol{c} = (0.767, 1.081, 1.410)^\top$

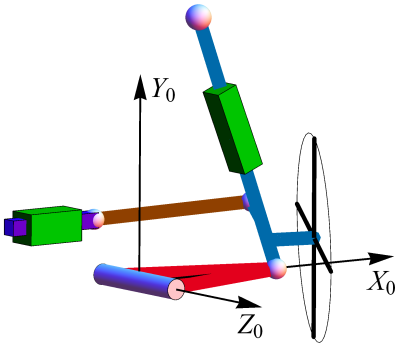

(b) $\boldsymbol{c} = (-1.662, -2.394, 1.441)^\top$

Fig. 12. Configurations corresponding to the real values of c_1, c_2, c_3 for $s = 50$mm, $y = -100$mm for Case-2

$p_{4y}^2 - p_{4z}^2 - s_x^2 - s_y^2 - s_z^2 + 2l_{3x}o_{1x} + 2l_{3y}o_{1y} - 2l_{3z}o_{1z} + 2o_{1x}p_{4x} - 2l_{3y}p_{4y} + 2o_{1y}p_{4y} + 2l_{3z}p_{4z} + 2o_{1x}s_x - 2p_{4x}s_x - 2l_{3x}(p_{4x} + s_x) - 2l_{3y}s_y + 2o_{1y}s_y - 2p_{4y}s_y + 2l_{3z}s_z - 2p_{4z}s_z)c_1 + c_3(-l_1^2 + l_4^2 - l_{3x}^2 - l_{3y}^2 - l_{3z}^2 - p_{4x}^2 - p_{4y}^2 - p_{4z}^2 - s_x^2 - s_y^2 - s_z^2 - 2l_{3y}o_{1y} - 2l_{3z}o_{1z} + 2o_{1x}p_{4x} + 2l_{3y}p_{4y} + 2o_{1y}p_{4y} + 2l_{3z}p_{4z} + 2o_{1x}s_x - 2p_{4x}s_x + 2l_{3x}(-o_{1x} + p_{4x} + s_x) + 2l_{3y}s_y + 2o_{1y}s_y - 2p_{4y}s_y + 2l_{3z}s_z - 2p_{4z}s_z)c_1 - 2c_2(2l_{3z}(o_{1y} - p_{4y} - s_y) + o_{1z}(p_{4y} + s_y) + 2l_{3y}(-o_{1z} + p_{4z} + s_z))c_1 + 2c_3^2 l_{3x}o_{1z} + o_{1z}(l_{3x} - p_{4x} - s_x) + c_2^4 o_{1z}(l_{3x} + p_{4x} + s_x) + c_3^4 o_{1z}(l_{3x} + p_{4x} + s_x) + 2c_2^2 c_3^2 o_{1z}(l_{3x} + p_{4x} + s_x) + c_2c_3(4l_{3y}(-o_{1x} + p_{4x} + s_x) + 4l_{3x}(o_{1y} - p_{4y} - s_y)) - 2c_3^3 o_{1z}(p_{4y} + s_y) - 2c_3 o_{1z}(p_{4y} + s_y) + c_2(l_1^2 - l_4^2 + l_{3x}^2 + l_{3y}^2 + l_{3z}^2 + p_{4x}^2 + p_{4y}^2 + p_{4z}^2 + s_x^2 + s_y^2 + s_z^2 + 2l_{3y}o_{1y} + 2l_{3z}o_{1z} - 2o_{1x}p_{4x} - 2l_{3y}p_{4y} - 2o_{1y}p_{4y} - 2l_{3z}p_{4z} + 2l_{3x}(o_{1x} - p_{4x} - s_x) - 2o_{1x}s_x + 2p_{4x}s_x - 2l_{3y}s_y - 2o_{1y}s_y + 2p_{4y}s_y - 2l_{3z}s_z + 2p_{4z}s_z) + c_2c_3^2(l_1^2 - l_4^2 + l_{3x}^2 + l_{3y}^2 + l_{3z}^2 + p_{4x}^2 + p_{4y}^2 + p_{4z}^2 + s_x^2 + s_y^2 + s_z^2 - 2l_{3y}o_{1y} + 2l_{3z}o_{1z} - 2o_{1x}p_{4x} + 2l_{3y}p_{4y} - 2o_{1y}p_{4y} - 2l_{3z}p_{4z} - 2o_{1x}s_x + 2p_{4x}s_x + 2l_{3x}(-o_{1x} + p_{4x} + s_x) + 2l_{3y}s_y - 2o_{1y}s_y + 2p_{4y}s_y - 2l_{3z}s_z + 2p_{4z}s_z) + c_2^3(l_1^2 - l_4^2 + l_{3x}^2 + l_{3y}^2 + l_{3z}^2 + p_{4x}^2 + p_{4y}^2 + p_{4z}^2 + s_x^2 + s_y^2 + s_z^2 + 2l_{3y}o_{1y} - 2l_{3z}o_{1z} - 2o_{1x}p_{4x} - 2l_{3y}p_{4y} - 2o_{1y}p_{4y} + 2l_{3z}p_{4z} - 2o_{1x}s_x + 2p_{4x}s_x + 2l_{3x}(-o_{1x} + p_{4x} + s_x) - 2l_{3y}s_y - 2o_{1y}s_y + 2p_{4y}s_y + 2l_{3z}s_z + 2p_{4z}s_z) - 2c_2^2c_3(o_{1x}(p_{4y} + s_y) + 2l_{3z}(-o_{1y} + p_{4y} + s_y) + 2l_{3y}(-o_{1z} + p_{4z} + s_z)) + c_2^2(4l_{3z}(o_{1x} - p_{4x} - s_x) - 2l_{3x}(o_{1z} - 2(p_{4z} + s_z)));$

$f_3(c_1, c_2, c_3) = c_3c_1^3(-l_{5y} + o_{1y} - p_{7y} - y) + c_2c_1^2(l_{5y} - o_{1y} + p_{7y} + y) + c_3^3c_1(-l_{5y} + o_{1y} - p_{7y} - y) + c_2^2c_3c_1(l_{5y} + o_{1y} - p_{7y} - y) + c_3c_1(l_{5y} + o_{1y} - p_{7y} - y) + c_2^3(-l_{5y} - o_{1y} + p_{7y} + y) + c_2(-l_{5y} - o_{1y} + p_{7y} + y) + c_2c_3^2(l_{5y} - o_{1y} + p_{7y} + y) + c_3c_1^2(-2l_{5z} - o_{1z}) + c_2c_3^2c_1(2l_{5z} - o_{1z}) + c_2c_1(2l_{5z} - o_{1z}) + c_2^2c_3(-2l_{5z} - o_{1z}) + c_2c_3c_1^2(2l_{5x} + 2r_2) + c_3^2c_1(2l_{5x} + 2r_2) + c_2^2c_1(-2l_{5x} - 2r_2) + c_2c_3(-2l_{5x} - 2r_2) - c_2c_1^3o_{1z} - c_2^3c_1o_{1z} - c_3^3o_{1z} - c_3o_{1z}.$

References

[1] ARIKERE, A., SARAVANA KUMAR, G., AND BANDYOPADHYAY, S. Optimisation of double wishbone suspension system using multi-objective genetic algorithm. In *SEAL*, vol. 6457 of *Lecture Notes in Computer Science*. Springer Berlin Heidelberg, 2010, pp. 445–454.

[2] ATTIA, H. Numerical kinematic analysis of the standard macpherson motor-vehicle suspension system. *KSME International Journal*

17, 12 (2003), 1961–1968.

[3] BANDYOPADHYAY, S., AND GHOSAL, A. Geometric characterization and parametric representation of the singularity manifold of a 6-6 stewart platform manipulator. *Mechanism and Machine Theory 41*, 11 (2006), 1377–1400.

[4] COX, D., LITTLE, J., AND O'SHEA, D. *Ideals, Varieties, and Algorithms: An Introduction to Computational Algebraic Geometry and Commutative Algebra*, 3rd. ed. Springer-Verlag, New York, 2007.

[5] CRONIN, D. Macpherson strut kinematics. *Mechanism and Machine Theory 16*, 6 (1981), 631–644.

[6] GHOSAL, A. *Robotics: Fundamental Concepts and Analysis*, 1st. ed. Oxford University Press, New Delhi, 2006.

[7] GREUEL, G.-M., AND PFISTER, G. *A Singular introduction to commutative algebra. With contributions by Olaf Bachmann, Christoph Lossen and Hans Schönemann*, 2nd. extended ed. Berlin: Springer, 2007.

[8] JÖRNSEN REIMPELL, H. S., AND BETZLER, J. W. *The Automotive Chassis: Engineering Principles*. SAE International, Warrendale, PA, 2001.

[9] MÁNTARAS, D. A., LUQUE, P., AND VERA, C. Development and validation of a three-dimensional kinematic model for the mcpherson steering and suspension mechanisms. *Mechanism and Machine Theory 39*, 6 (2004), 603–619.

[10] PAPEGAY, Y. A., MERLET, J.-P., AND DANEY, D. Exact kinematics analysis of cars suspension mechanisms using symbolic computation and interval analysis. *Mechanism and Machine Theory 40*, 4 (2005), 395–413.

[11] SELIG, J. M. *Geometric fundamentals of robotics*, 2nd. ed. Springer, New York, 1996.

[12] WOLFRAM, S. *The Mathematica Book*. Cambridge University Press, Cambridge, 2004.